

Viscous heating and instability of the adiabatic buoyant flows in a horizontal channel

A. Barletta*; M. Celli

Department of Industrial Engineering, Alma Mater Studiorum Università di Bologna,
Viale Risorgimento 2, 40136 Bologna, Italy

D. A. S. Rees

Department of Mechanical Engineering, University of Bath, Bath BA2 7AY, U.K.

February 2, 2023

Abstract

The stability of buoyant flows occurring in the mixed convection regime for a viscous fluid in a horizontal plane-parallel channel with adiabatic walls is investigated. The basic flow features a parallel velocity field under stationary state conditions. There exists a duality of flows, for every prescribed value of the mass flow rate across the channel cross-section, caused by the combined actions of viscous dissipation and of the buoyancy force. As pointed out in a previous study, only the primary branch of the dual solutions is compatible with the Oberbeck-Boussinesq approximation. Thus, the stability analysis will be focussed on the stability of such flows. The onset of the thermal instability with small-amplitude perturbations of the basic flow is investigated by assuming a very large Prandtl number, which is equivalent to a creeping flow regime. The neutral stability curves and the critical parametric conditions for the onset of instability are determined numerically.

Keywords: Viscous heating, Mixed Convection, Dual flows, Linear stability, Newtonian fluid, Adiabatic walls.

*Corresponding author: antonio.barletta@unibo.it

1 Introduction

The instability of stationary and fully-developed flows in a plane channel is a classical topic discussed in a plethora of textbooks on fluid mechanics. Among the many, we mention Drazin and Reid [1] and Kundu et al. [2]. The instability arises as hydrodynamic in nature when there is no thermal forcing on the flow via the boundary conditions, with the critical conditions for linear instability being determined through the solution of the Orr-Sommerfeld eigenvalue problem [1, 2]. A different conclusion is drawn when, even in the absence of an external temperature difference between the plane boundary walls, the frictional heating associated with the viscous flow is taken into account. In this case, the thermally-induced instability acts via a temperature coupling term in the local momentum balance equation. Such a term can be the viscous force as the fluid viscosity is temperature-dependent [3, 4]. An alternative scenario is the buoyancy effect, where the temperature coupling term in the momentum balance is the gravity force with a temperature-dependent fluid density modelled according to the Oberbeck-Boussinesq approximation [5–15].

The combined effects of buoyancy and viscous heating may yield situations where the stationary flows in a channel or duct caused by a given dynamic input, either a prescribed pressure gradient or a prescribed mass flow rate, are dual. The duality is usually accompanied by a merging between the solution branches which produces a maximum parametric condition in terms of either pressure gradient or mass flow rate above which no stationary flow is possible. This behaviour is widely documented in the literature [8–10, 12, 16–18]. We mention that dual or, more generally, multiple solutions are a consequence of the nonlinearity of buoyant flows and their existence does not necessarily imply the inclusion of the viscous dissipation term in the local energy balance equation [19, 20].

The aim of this paper is the stability analysis of the primary branch of dual solutions found by Barletta et al. [18]. In fact, these authors pointed out that the secondary branch refers to conditions hardly compatible with the Oberbeck-Boussinesq approximation scheme underlying their determination. The flow conditions employed in this analysis involve the fully-developed regime in a horizontal channel with thermally insulated walls. The interplay between the buoyancy force and the viscous heating of the channel flow leads to a mixed convection scenario where the velocity displays a departure from the Poiseuille profile, with a duality of solutions for every prescribed mass flow rate across the channel. Though widely described in Barletta et al. [18], the main features of the dual flows are surveyed also in this paper for self-containedness of our presentation and for a precise definition of which basic flow we assume when testing the transition to instability. The character of our stability analysis reflects a similar study published some years ago and relative to Darcy’s flow in a fluid-saturated porous material [21]. As we are interested in the destabilising action of the viscous dissipation term in the energy balance, we will assume high viscosity and low diffusivity properties of the fluid, which means a very large Prandtl number. This assumption simplifies the governing equations for the perturbations of the basic solution as they are formulated for a creeping flow scheme with the inertial term in the momentum balance turning out to be negligible. A similar approach was followed also in Barletta and Nield [5] and in Barletta et al. [6]. The focus on the creeping flow regime makes our analysis completely different from the hydrodynamically combined stability analysis of the Poiseuille flow as based on the Orr-Sommerfeld eigenvalue problem. In fact, the hydrodynamic instability is relative to a condition where the inertial term of the momentum balance becomes utterly important for the emergence of the flow instability so that, in that case, the creeping flow scheme is inadequate [1, 2].

An important governing parameter in the forthcoming analysis is the Gebhart number, Ge .

This parameter is often employed in the literature where buoyant flows are studied by including the effect of viscous dissipation, though several authors prefer calling this parameter dissipation number, Di . Indeed, the definitions of Ge and Di are the same. The former symbol is a recognition of the pioneering study by Gebhart [22], while the latter is still widely employed in the literature on geophysical flows. Among the many studies regarding the geophysical applications of the natural convection heat transfer with viscous heating, we mention the interesting papers by Kincaid and Silver [23] and by van den Berg and Yuen [24]. The paper by Kincaid and Silver [23] provides a model where the excess heat generated in the upper part of Earth mantle during orogenesis is attributed to a viscous dissipation contribution, envisaging also cases where Di is as large as 6. In van den Berg and Yuen [24] the assumption $Di = 0.7$ is made on studying buoyant flows in the mantle by including the effect of viscous dissipation coupled also with the internal heating due to radioactivity and the adiabatic work induced by compression/decompression processes.

2 Mathematical Model

Let us consider a Newtonian fluid flowing in a plane-parallel channel bounded by walls at $z = 0$ and $z = H$. The horizontal x and y directions are unbounded, while the uniform gravitational acceleration is given by $\mathbf{g} = -g\hat{\mathbf{e}}_z$, where g is the modulus of \mathbf{g} and $\hat{\mathbf{e}}_z$ is the unit vector of the z axis. The boundary walls are both rigid and with a perfect thermal insulation.

2.1 Governing Equations

The Oberbeck-Boussinesq approximation can be employed so that the governing equations are written as,

$$\nabla \cdot \mathbf{u} = 0, \quad (1a)$$

$$\frac{\partial \mathbf{u}}{\partial t} + (\mathbf{u} \cdot \nabla) \mathbf{u} = -\frac{1}{\rho} \nabla p + g\beta(T - T_0) \hat{\mathbf{e}}_z + \nu \nabla^2 \mathbf{u}, \quad (1b)$$

$$\frac{\partial T}{\partial t} + (\mathbf{u} \cdot \nabla) T = \alpha \nabla^2 T + \frac{\nu}{c} \Phi, \quad (1c)$$

where ρ , β , ν , α and c are the fluid density, thermal expansion coefficient, kinematic viscosity, thermal diffusivity and specific heat evaluated at the constant reference temperature T_0 . In Eqs. (1), \mathbf{u} is the velocity, p is the local difference between the pressure and the hydrostatic pressure, T is the temperature and t is the time. Hereafter, p is called the pressure field for brevity. The symbol Φ denotes the dissipation function which, according to Einstein's notation for the implicit sums over repeated indices, can be expressed as

$$\Phi = \frac{1}{2} \gamma_{ij} \gamma_{ij} \quad \text{using} \quad \gamma_{ij} = \frac{\partial u_i}{\partial x_j} + \frac{\partial u_j}{\partial x_i}. \quad (2)$$

In Eq. (2), γ_{ij} is the shear rate tensor, while u_i and x_i denote the i th Cartesian components of the velocity vector $\mathbf{u} = (u, v, w)$ and of the position vector $\mathbf{x} = (x, y, z)$.

The boundary conditions imposed at $z = 0, H$ express impermeability, no-slip and adiabaticity,

$$\mathbf{u} = 0, \quad \frac{\partial T}{\partial z} = 0 \quad \text{for} \quad z = 0, H. \quad (3)$$

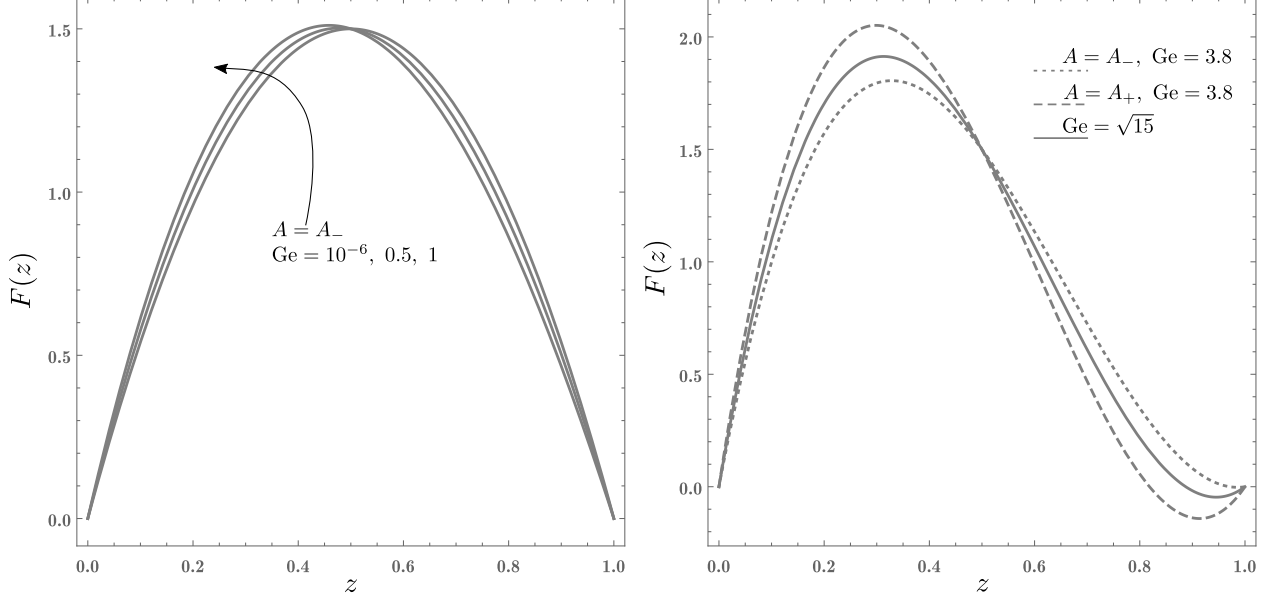


Figure 1: Plots of $F(z)$ for either $A = A_-$ or $A = A_+$ with different values of Ge

2.2 Dimensionless Formulation

Dimensionless quantities can be defined through the scaling

$$\begin{aligned} \frac{\mathbf{x}}{H} \rightarrow \mathbf{x}, \quad \frac{t}{H^2/\alpha} \rightarrow t, \quad \frac{\mathbf{u}}{\alpha/H} \rightarrow \mathbf{u}, \quad \frac{p}{\rho\alpha\nu/H^2} \rightarrow p \\ \frac{T - T_0}{\Delta T} \rightarrow T, \quad \frac{\Phi}{\alpha^2/H^4} \rightarrow \Phi \quad \text{using} \quad \Delta T = \frac{\alpha\nu}{g\beta H^3}. \end{aligned} \quad (4)$$

On account of Eq. (4), Eqs. (1) and (3) can be rewritten in a dimensionless form as

$$\nabla \cdot \mathbf{u} = 0, \quad (5a)$$

$$\frac{1}{Pr} \left[\frac{\partial \mathbf{u}}{\partial t} + (\mathbf{u} \cdot \nabla) \mathbf{u} \right] = -\nabla p + T \hat{\mathbf{e}}_z + \nabla^2 \mathbf{u}, \quad (5b)$$

$$\frac{\partial T}{\partial t} + (\mathbf{u} \cdot \nabla) T = \nabla^2 T + Ge \Phi, \quad (5c)$$

with

$$\mathbf{u} = 0, \quad \frac{\partial T}{\partial z} = 0 \quad \text{for} \quad z = 0, 1. \quad (6)$$

In Eqs. (5b) and (5c), the Prandtl number, Pr , and the Gebhart number, Ge , are defined as

$$Pr = \frac{\nu}{\alpha}, \quad Ge = \frac{g\beta H}{c}. \quad (7)$$

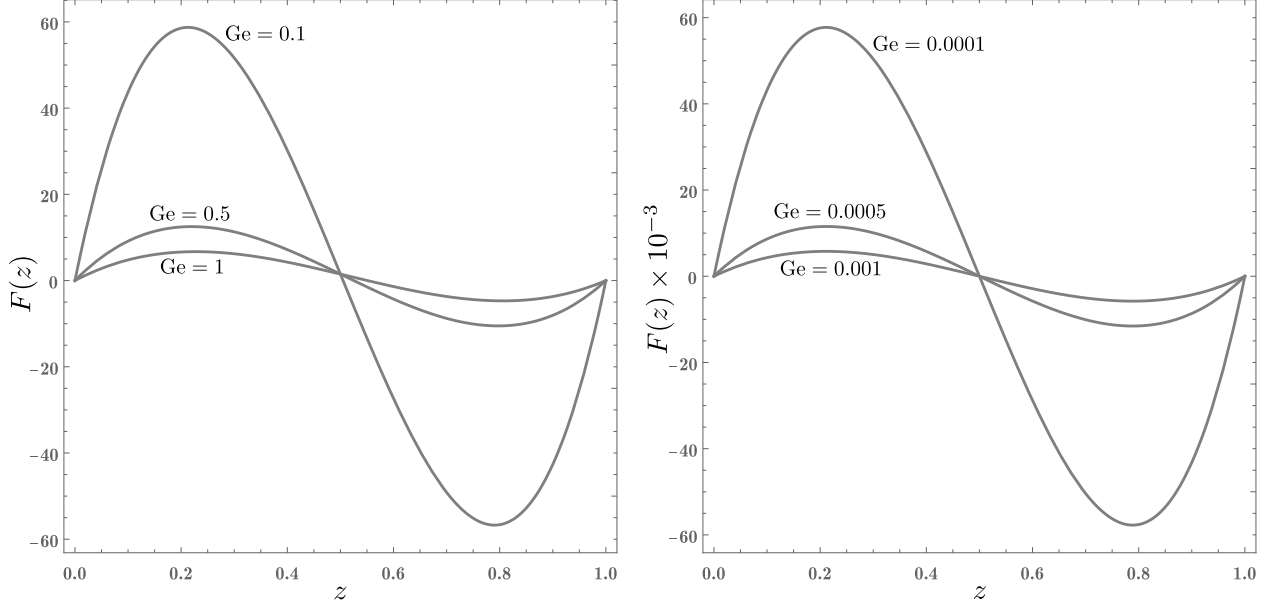


Figure 2: Plots of $F(z)$ for $A = A_+$ with different values of Ge

3 Basic Dual Flows

In this section, we survey the main features of the dual adiabatic flows relying on the results conveyed in a previous study [18]. Stationary solutions of Eqs. (5) and (6) with a parallel velocity field can be expressed as

$$\begin{aligned}
 u_b &= Pe F(z) \cos \varphi, & v_b &= Pe F(z) \sin \varphi, & w_b &= 0, \\
 T_b &= Pe F'''(z) (x \cos \varphi + y \sin \varphi) + Pe^2 G(z), \\
 \nabla p_b &= \left(Pe F''(z) \cos \varphi, Pe F''(z) \sin \varphi, T_b \right),
 \end{aligned} \tag{8}$$

where the subscript b indicates “basic solution”, Pe is the Péclet number and the primes denote the derivatives with respect to z , while functions $F(z)$ and $G(z)$ are polynomials given by

$$\begin{aligned}
 F(z) &= z(1-z)[A - 2(A-6)z], \\
 G(z) &= \frac{z^2}{10} \left\{ -5A^2 Ge + 20A[(A-4)Ge + A-6]z \right. \\
 &\quad \left. - 10[A^2(4Ge+3) - 30A(Ge+1) + 48Ge+72]z^2 \right. \\
 &\quad \left. + 12(A-6)[3(A-4)Ge + A-6]z^3 - 12(A-6)^2 Ge z^4 \right\}.
 \end{aligned} \tag{9}$$

The constant A can be equal either to A_- or A_+ , where

$$A_- = 2 \frac{3Ge + 15 - \sqrt{15(15 - Ge^2)}}{Ge}, \quad A_+ = 2 \frac{3Ge + 15 + \sqrt{15(15 - Ge^2)}}{Ge}. \tag{10}$$

Equations (8)-(10) describe horizontal parallel flows in the xy plane where the velocity field is inclined an angle φ to the x axis. The twofold expression of $A = A_{\pm}$ means that there are dual

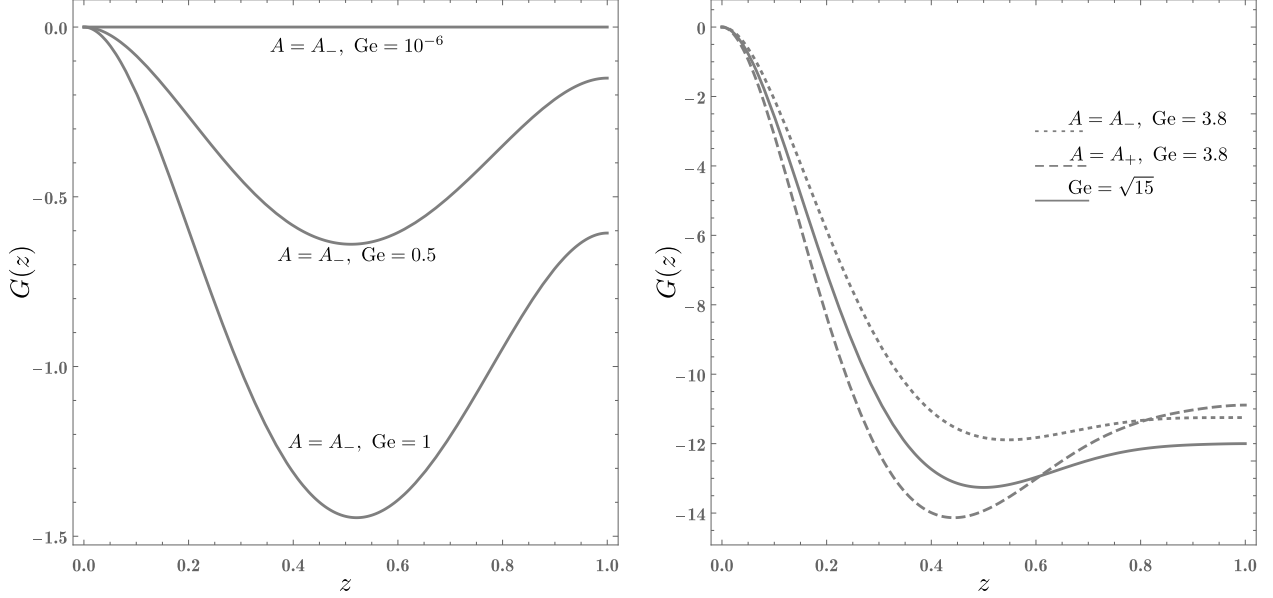


Figure 3: Plots of $G(z)$ for either $A = A_-$ or $A = A_+$ with different values of Ge

flows corresponding to the same prescribed Péclet and Gebhart numbers. Such dual flows exist if $Ge \leq \sqrt{15} \approx 3.87298$ and they coincide only when $Ge = \sqrt{15}$. We note that such an upper bound for Ge is an extremely large value in practical cases [18]. The Péclet number is defined in terms of dimensional quantities as

$$Pe = \frac{U_0 H}{\alpha}, \quad (11)$$

where the reference dimensional velocity U_0 is intended as the basic average velocity in the horizontal flow direction defined by the unit vector $(\cos \varphi, \sin \varphi, 0)$. In fact, Eq. (9) yields

$$\int_0^1 F(z) dz = 1, \quad (12)$$

which means that the average dimensionless velocity in the flow direction is equal to Pe .

It is to be mentioned that function $G(z)$ is defined only up to an arbitrary additive constant which, in Eq. (9), has been fixed so that $G(0) = 0$. Such a feature is due to the Neumann boundary conditions for the temperature which leave this constant undetermined. The temperature appears on the right hand side of Eq. (5b) next to the ∇p term. Thus, changing the temperature by an additive constant has the physical meaning of changing the reference temperature value employed for the formulation of the Oberbeck-Boussinesq approximation. This change leads to a redetermination of the hydrostatic pressure and to a resulting modification in the dimensional field p which, by definition, is the difference between the pressure and the hydrostatic pressure. In fact, the hydrostatic pressure is $-\rho g z$, where ρ is the fluid density evaluated at the reference temperature T_0 . It becomes clear that altering the arbitrary additive constant in $G(z)$ influences the basic solution only by modifying, through an overall additive constant, the local values of T_b

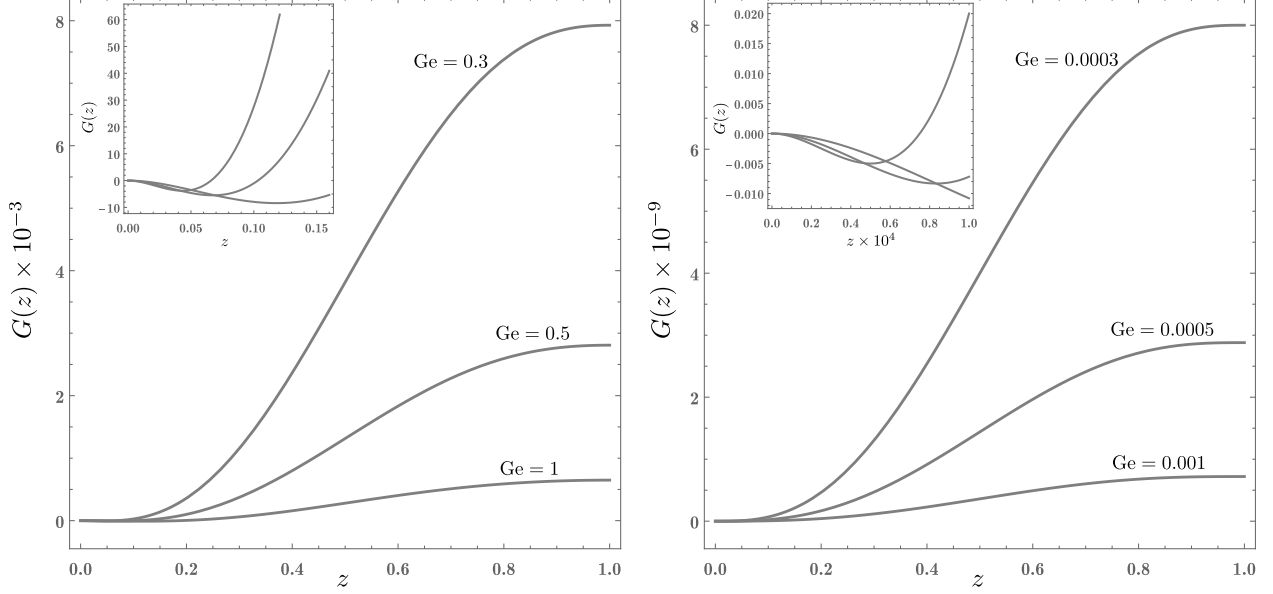


Figure 4: Plots of $G(z)$ for $A = A_+$ with different values of Ge

and, as a consequence of Eq. (9), also of $\partial p_b / \partial z$. On the other hand, the discussion of the stability of the dual basic flows, to be carried out later on, is not affected in any way by the choice of the arbitrary additive constant in the expression of $G(z)$. In fact, it will be shown that the dynamics of perturbations is governed by partial differential equations where ∇p_b is absent and T_b is present only through its gradient.

The physical effects underlying the basic dual solutions are the imposed horizontal flow rate causing the viscous heating and the buoyancy force induced by the resulting temperature gradient. Such effects become inactive when $Ge \rightarrow 0$, as highlighted by Eq. (5c), and the basic solution becomes an isothermal Poiseuille flow. This conclusion is made evident by taking the power series expansions of A_+ and A_- at small Ge ,

$$A_- = 6 + Ge + \mathcal{O}(Ge^2), \quad A_+ = \frac{60}{Ge} + 6 - Ge + \mathcal{O}(Ge^2). \quad (13)$$

Equation (13) yields $A_- = 6$, when $Ge \rightarrow 0$, while A_+ becomes singular. Hence, the A_+ -branch of the dual flows blows up when $Ge \rightarrow 0$, while the A_- -branch yields

$$\begin{aligned} u_b &= 6 Pe z (1 - z) \cos \varphi, & v_b &= 6 Pe z (1 - z) \sin \varphi, & w_b &= 0, \\ T_b &= 0, & \nabla p_b &= \left(-12 Pe \cos \varphi, -12 Pe \sin \varphi, 0 \right). \end{aligned} \quad (14)$$

Equation (14) represents the isothermal Poiseuille flow in the direction defined by the unit vector $(\cos \varphi, \sin \varphi, 0)$.

We note that, in every case where $Ge \neq 0$, the basic temperature gradient is inclined to the horizontal with constant horizontal components in the x and y directions. This feature is easily spotted by reckoning from Eq. (9) that $F'''(z) = 12(A - 6)$.

Figures 1 and 2 illustrate the velocity profiles as plots of $F(z)$ for various Gebhart numbers and for both branches $A = A_-$ and $A = A_+$. The $A = A_-$ branch shows very small departures

from the Poiseuille profile unless the Gebhart number becomes huge, namely, close to its upper bound $Ge = \sqrt{15}$. This feature is clearly visible in Fig. 1, while Fig. 2 reveals that the $A = A_+$ branch marks a sharp departure from the Poiseuille profile especially at small Gebhart numbers. The characteristics of the $A = A_+$ profiles show a bidirectional nature of the flow which arises also, albeit in a minimal way, for the $A = A_-$ profiles, but only when Ge is very close to its upper bound $\sqrt{15}$. Figure 2 also shows that, at small Gebhart numbers, $F(z)$ for the $A = A_+$ branch scales proportionally to Ge^{-1} , approximately. This feature is easily recognised on comparing the left-hand frame and the right-hand frame of Fig. 2, and it is proved on expanding $F(z)$ in a power series of Ge for $A = A_+$,

$$F(z) = \frac{60z(1-z)(1-2z)}{Ge} + 6(1-z)z + \mathcal{O}(Ge). \quad (15)$$

The vertical change of the basic temperature field is illustrated in Figs. 3 and 4 by plotting function $G(z)$ with different values of Ge for the $A = A_-$ and $A = A_+$ branches. Figure 3 shows that the $A = A_-$ branch features a significant dependence of the temperature profiles on Ge , despite the weak influence of the Gebhart number on the velocity profiles as already pointed out while commenting on Fig. 1. Figure 4 shows that, at small Ge and for the $A = A_+$ branch, function $G(z)$ scales proportionally to Ge^{-2} , approximately. This behaviour is shown through a power series expansion of $G(z)$ with $A = A_+$,

$$G(z) = \frac{720z^3(6z^2 - 15z + 10)}{Ge^2} - \frac{360z^2(1-z)^2(12z^2 - 12z + 5)}{Ge} + 72z^2(4z^3 - 10z^2 + 10z - 5) + \mathcal{O}(Ge). \quad (16)$$

A remarkable feature revealed by Fig. 3 is the unstable thermal stratification ($\partial T_b/\partial z < 0$) for the $A = A_-$ branch occurring at the lower part of the channel. Such an unstable thermal stratification does emerge for all Gebhart numbers also with the $A = A_+$ branch, although it can be visualised in Fig. 4 only through the miniatures at small values of z . Analytically, this conclusion can be inferred by evaluating $G''(0)$ with $A = A_+$,

$$G''(0) = - \frac{24 \left[(Ge + 5) \sqrt{15(15 - Ge^2)} + Ge(15 - Ge) + 75 \right]}{Ge}. \quad (17)$$

The right hand side of Eq. (17) is evidently negative for every $Ge \leq \sqrt{15}$. As a consequence, there always exist regions close to $z = 0$ where $G'(z) < 0$.

The existence of a region inside the channel with a negative z component of the basic temperature gradient for either the $A = A_-$ branch or the $A = A_+$ branch discloses the possibility of a thermal instability of the Rayleigh-Bénard type (heating from below) for the dual basic flows. This circumstance will be explored later on. It is to be mentioned that the vertical component of the basic temperature gradient is not the only source of a possible thermal instability. In fact, the constant horizontal components of ∇T_b may contribute possibly leading to a thermal instability of the Hadley-type.

It has been pointed out that the $A = A_+$ branch can hardly be considered compatible with the Oberbeck-Boussinesq approximate model underlying the existence of the dual solutions [18]. The reason is that the approximate model requires the product between the thermal expansion coefficient β and the maximum temperature difference across the flow domain to be much smaller

than unity. As pointed out by Barletta et al. [18], this condition is precluded when considering the $A = A_+$ branch of the dual solutions. On account of these findings, the forthcoming stability analysis will be focussed just on the $A = A_-$ branch.

4 Dynamics of small-amplitude perturbations

Let us perturb the basic dual flows,

$$\begin{pmatrix} \mathbf{u} \\ p \\ T \end{pmatrix} = \begin{pmatrix} \mathbf{u}_b \\ p_b \\ T_b \end{pmatrix} + \varepsilon \begin{pmatrix} \mathbf{U} \\ P \\ \Theta \end{pmatrix}, \quad (18)$$

where ε is the perturbation parameter and (\mathbf{U}, P, Θ) are the perturbations of velocity, pressure and temperature, respectively. The Cartesian components of \mathbf{U} are denoted as (U, V, W) . Let us substitute Eq. (18) into Eqs. (5) and (6) by employing Eqs. (2) and (8), namely

$$\nabla \cdot \mathbf{U} = 0, \quad (19a)$$

$$\frac{1}{\text{Pr}} \left[\frac{\partial \mathbf{U}}{\partial t} + (\mathbf{u}_b \cdot \nabla) \mathbf{U} + (\mathbf{U} \cdot \nabla) \mathbf{u}_b \right] = -\nabla P + \Theta \hat{\mathbf{e}}_z + \nabla^2 \mathbf{U}, \quad (19b)$$

$$\frac{\partial \Theta}{\partial t} + (\mathbf{u}_b \cdot \nabla) \Theta + (\mathbf{U} \cdot \nabla) T_b = \nabla^2 \Theta + 2 \text{Ge} \left[\left(\frac{\partial U}{\partial z} + \frac{\partial W}{\partial x} \right) u'_b + \left(\frac{\partial V}{\partial z} + \frac{\partial W}{\partial y} \right) v'_b \right], \quad (19c)$$

$$\mathbf{U} = 0, \quad \frac{\partial \Theta}{\partial z} = 0 \quad \text{for } z = 0, 1, \quad (19d)$$

where terms $\mathcal{O}(\varepsilon^2)$ have been neglected in order to account for small-amplitude perturbations.

Since the basic flow direction is inclined an angle φ to the x direction, the x axis defines an arbitrary horizontal direction, so that the normal modes of perturbation can be expressed as plane waves propagating along the x -direction. The effect of arbitrary oblique modes can be tested by allowing a changing angle within the range $0 \leq \varphi \leq \pi/2$. The values $\varphi = 0$ and $\varphi = \pi/2$ yield the transverse modes and the longitudinal modes, respectively. Thus, we write

$$\begin{pmatrix} \mathbf{U} \\ P \\ \Theta \end{pmatrix} = \begin{pmatrix} \hat{\mathbf{U}}(z) \\ \hat{P}(z) \\ \hat{\Theta}(z) \end{pmatrix} e^{i k x} e^{\lambda t}, \quad (20)$$

where k is the real-valued wavenumber, while λ is a complex-valued parameter. The real and imaginary parts of λ are denoted as $\lambda = \eta - i\omega$, with η expressing the growth rate and ω yielding the angular frequency. Linear instability is identified with the condition $\eta > 0$, while $\eta = 0$ expresses the threshold case of neutral stability. We substitute Eq. (20) into Eqs. (19), so that we can write

$$i k \hat{U} + \hat{W}' = 0, \quad (21a)$$

$$\frac{1}{\text{Pr}} \left(\lambda \hat{U} + i k u_b \hat{U} + \hat{W} u'_b \right) = -i k \hat{P} + \hat{U}'' - k^2 \hat{U}, \quad (21b)$$

$$\frac{1}{\text{Pr}} \left(\lambda \hat{V} + i k u_b \hat{V} + \hat{W} v'_b \right) = \hat{V}'' - k^2 \hat{V}, \quad (21c)$$

$$\frac{1}{\text{Pr}} \left(\lambda \hat{W} + i k u_b \hat{W} \right) = -\hat{P}' + \hat{\Theta} + \hat{W}'' - k^2 \hat{W}, \quad (21d)$$

$$\lambda \hat{\Theta} + i k u_b \hat{\Theta} + \hat{U} \frac{\partial T_b}{\partial x} + \hat{V} \frac{\partial T_b}{\partial y} + \hat{W} \frac{\partial T_b}{\partial z} = \hat{\Theta}'' - k^2 \hat{\Theta} + 2 \text{Ge} \left[(\hat{U}' + i k \hat{W}) u'_b + \hat{V}' v'_b \right], \quad (21e)$$

$$\hat{U} = 0, \quad \hat{V} = 0, \quad \hat{W} = 0, \quad \hat{\Theta}' = 0 \quad \text{for } z = 0, 1, \quad (21f)$$

where $(\hat{U}, \hat{V}, \hat{W})$ are the Cartesian components of $\hat{\mathbf{U}}$.

The physically significant situation where the viscous dissipation effect is expected to cause the instability is when the fluid has a large kinematic viscosity combined with a small thermal diffusivity. Roughly speaking, such fluids are markedly susceptible to frictional heating while the diffusion of such an internally generated heat is inefficient. This situation reasonably occurs when the Prandtl number is extremely large.

4.1 Creeping Flow

A regime of creeping flow occurs when the inertial terms in the momentum balance are negligible. This happens when the limit $\text{Pr} \rightarrow \infty$ is taken for Eq. (19b). As mentioned above, such a limit identifies a condition where an extremely viscous fluid is employed having a small thermal diffusivity. In this limit, Eqs. (21) simplify to

$$i k \hat{U} + \hat{W}' = 0, \quad (22a)$$

$$-i k \hat{P} + \hat{U}'' - k^2 \hat{U} = 0, \quad (22b)$$

$$\hat{V}'' - k^2 \hat{V} = 0, \quad (22c)$$

$$-\hat{P}' + \hat{\Theta} + \hat{W}'' - k^2 \hat{W} = 0, \quad (22d)$$

$$\lambda \hat{\Theta} + i k u_b \hat{\Theta} + \hat{U} \frac{\partial T_b}{\partial x} + \hat{V} \frac{\partial T_b}{\partial y} + \hat{W} \frac{\partial T_b}{\partial z} = \hat{\Theta}'' - k^2 \hat{\Theta} + 2 \text{Ge} \left[(\hat{U}' + i k \hat{W}) u'_b + \hat{V}' v'_b \right], \quad (22e)$$

$$\hat{U} = 0, \quad \hat{V} = 0, \quad \hat{W} = 0, \quad \hat{\Theta}' = 0 \quad \text{for } z = 0, 1. \quad (22f)$$

From Eqs. (22c) and (22f), one can immediately conclude that $\hat{V} = 0$ in the whole range $0 \leq z \leq 1$. Furthermore, by employing Eqs. (22a) and (22b), one can express \hat{U} and \hat{P} in terms of \hat{W} and its derivatives. Thus, one is led to a reformulation of Eqs. (22) involving only the unknowns \hat{W} and $\hat{\Theta}$,

$$\hat{W}'''' - 2 k^2 \hat{W}'' + k^4 \hat{W} - k^2 \hat{\Theta} = 0, \quad (23a)$$

$$\hat{\Theta}'' - [k^2 + \lambda + i k \text{Pe} F(z) \cos \varphi] \hat{\Theta} + \frac{2 i \text{Ge} \text{Pe} F'(z) \cos \varphi}{k} (\hat{W}'' + k^2 \hat{W}) - \frac{i \text{Pe} F'''(z) \cos \varphi}{k} \hat{W}' - \text{Pe}^2 G'(z) \hat{W} = 0, \quad (23b)$$

$$\hat{W} = 0, \quad \hat{W}' = 0, \quad \hat{\Theta}' = 0 \quad \text{for } z = 0, 1. \quad (23c)$$

Creeping flow is usually associated with a regime of extremely small Reynolds number, $\text{Re} = \text{Pe}/\text{Pr}$. From the mathematical viewpoint, creeping flow means a situation where the limit $\text{Re} \rightarrow 0$ is combined with the limit $\text{Pr} \rightarrow \infty$. These limits can be taken on keeping $\text{Pe} = \text{Re} \text{Pr} \sim O(1)$. In the

following, we will consider the dynamics of perturbations as modelled by a creeping flow achieved with a finite Péclet number.

The linear analysis of the instability for the basic flows defined by Eqs. (8)-(10) is carried out by solving numerically the eigenvalue problem (23). The solution is sought by fixing the input parameters (φ, Ge) and by determining the neutral stability threshold value of Pe versus the wavenumber k . The angular frequency, ω , of the neutrally stable modes is also determined.

The neutral stability threshold implies a zero growth rate, η . Additionally, for the sake of convenience, the basic average velocity is taken into account by redefining the angular frequency in the comoving reference frame, namely

$$\hat{\omega} = \omega - k \text{Pe} \cos \varphi. \quad (24)$$

Thus, Eqs. (23) can be rewritten as

$$\hat{W}'''' - 2k^2 \hat{W}'' + k^4 \hat{W} - k^2 \hat{\Theta} = 0, \quad (25a)$$

$$\hat{\Theta}'' - \left[k^2 - i\hat{\omega} + ik \text{Pe} \hat{F}(z) \cos \varphi \right] \hat{\Theta} + \frac{2i \text{Ge} \text{Pe} \hat{F}'(z) \cos \varphi}{k} (\hat{W}'' + k^2 \hat{W}) - \frac{i \text{Pe} \hat{F}'''(z) \cos \varphi}{k} \hat{W}' - \text{Pe}^2 G'(z) \hat{W} = 0, \quad (25b)$$

$$\hat{W} = 0, \quad \hat{W}' = 0, \quad \hat{\Theta}' = 0 \quad \text{for } z = 0, 1, \quad (25c)$$

where $\hat{F}(z) = F(z) - 1$ is a function with a zero average value over the interval $0 \leq z \leq 1$, as a consequence of Eq. (12). By assigning φ as an input datum for the solution of Eqs. (25), one actually defines the type of oblique modes perturbing the flow, with the transverse modes ($\varphi = 0$) and the longitudinal modes ($\varphi = \pi/2$) as limiting cases.

5 Discussion of the Results

We pointed out in Section 3 that the linear stability analysis is relative to the $A = A_-$ branch of the dual flows. The numerical solution of the stability eigenvalue problem (25) is sought by employing the shooting method. We do not go into the details of this numerical technique as its use for the solution of flow stability eigenvalue problems has been widely discussed elsewhere [25, 26].

The software tool actually employed to implement the shooting method is *Mathematica* (© Wolfram Research, Inc.) with its functions `NDSolve` and `FindRoot`. The former function serves to solve the initial value problem based on Eqs. (25), starting at $z = 0$, while the latter function solves the target conditions (25c) at $z = 1$, thus yielding the numerical values for the neutral stability output data ($\hat{\omega}, \text{Pe}$). The neutral stability condition is represented by the curve in the parametric (k, Pe) plane, with the minimum Pe point along the curve yielding the critical condition for the onset of instability. Such a critical condition is given by $k = k_c$ and $\text{Pe} = \text{Pe}_c$, where the subscript c stands for critical value. Tracing the dependence of Pe_c on the inclination angle φ of the perturbation mode in different cases allows one to establish which modes are the most effective at onset of instability. Then, the stability analysis can be focussed just on those modes.

5.1 The Most Unstable Perturbations

We start the stability analysis from high values of Ge , namely $\text{Ge} = \sqrt{15}$ and $\text{Ge} = 2$. The neutral stability curves in the (k, Pe) plane are drawn in Fig. 5 for the transverse and the longitudinal

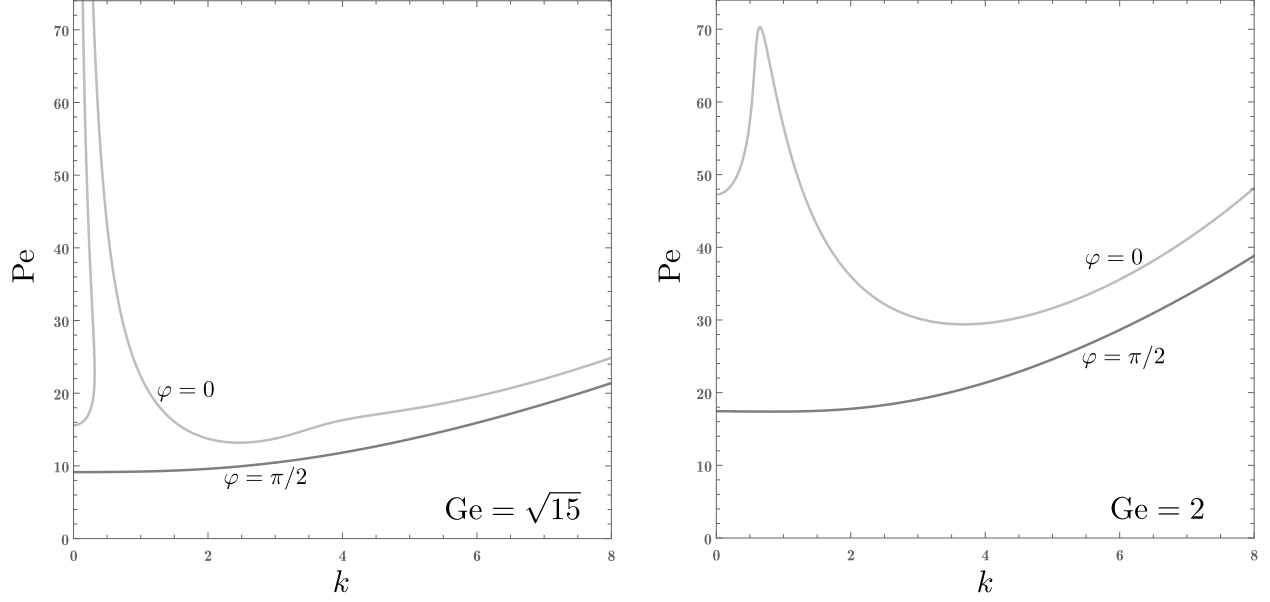


Figure 5: Neutral stability curves in the (k, Pe) plane for transverse (light grey line, $\varphi = 0$) and longitudinal (dark grey line, $\varphi = \pi/2$) modes

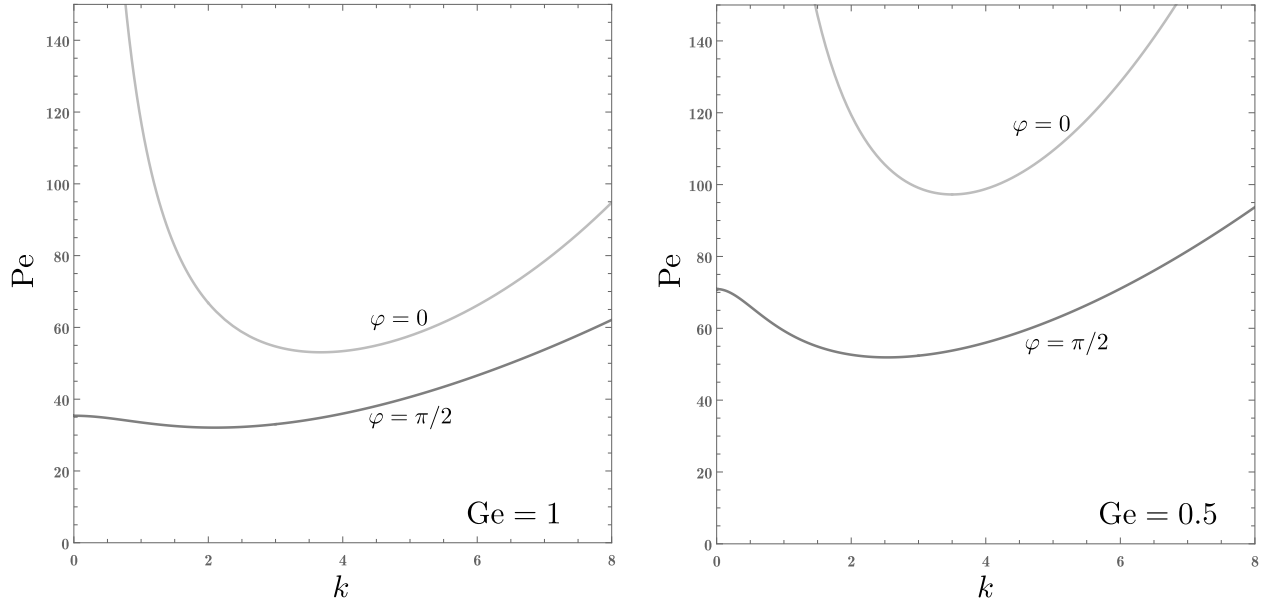


Figure 6: Neutral stability curves in the (k, Pe) plane for transverse (light grey line, $\varphi = 0$) and longitudinal (dark grey line, $\varphi = \pi/2$) modes

modes. We point out that $Ge = \sqrt{15}$ is the highest possible value of the Gebhart number. In fact, such a value is the highest possible according to the mathematical definition of the dual solutions, but we stress that this value is extremely large for physical systems. Figure 5 reveals that, both for $Ge = \sqrt{15}$ and $Ge = 2$, the longitudinal modes are the more unstable as they yield the transition

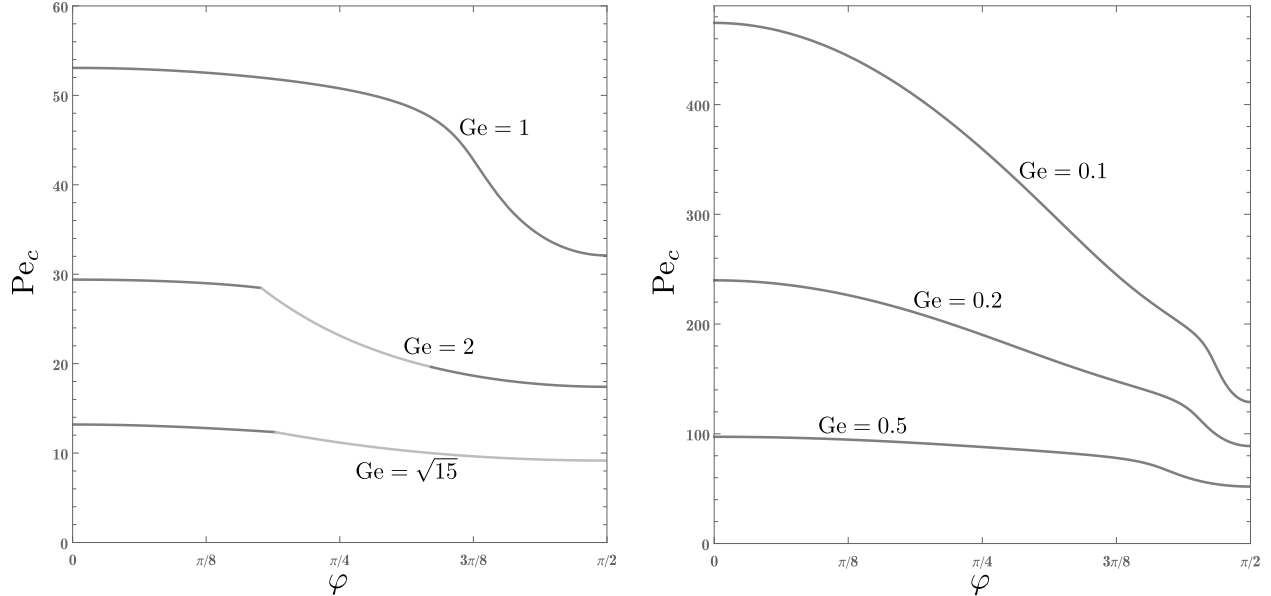


Figure 7: Critical values of Pe versus φ for oblique modes. Light grey lines denote $k_c = 0$ critical conditions, while dark grey lines denote $k_c \neq 0$ critical conditions

to instability with lower values of Pe for every k . The neutral stability curves for longitudinal modes reveal also that a finite value of Pe is achieved when $k \rightarrow 0$. This feature has been observed also in the study of the Rayleigh-Bénard instability when Neumann boundary conditions for the temperature are utilised, instead of the usual Dirichlet temperature conditions [27]. We point out that the critical value of Pe for longitudinal modes is obtained for $k \rightarrow 0$ in the case $Ge = \sqrt{15}$, but for a nonzero k with $Ge = 2$ though hardly evident in Fig. 5. More precisely, one finds

$$k_c = 0.842235, \quad Pe_c = 17.4116, \quad \text{for } Ge = 2. \quad (26)$$

We also note that the neutral stability curve for transverse modes is disconnected in two parts when $Ge = \sqrt{15}$. These disconnected parts join in a single curve when $Ge = 2$, thus forming a local maximum of Pe versus k .

The conclusion that longitudinal modes are the most unstable is confirmed by Fig. 6 which is relative to $Ge = 1$ and $Ge = 0.5$. For both values of Ge , the critical condition $Pe = Pe_c$ occurs for longitudinal modes with a nonzero k_c . There is a markedly different shape of the neutral stability curves for transverse modes with $Ge = 1$ and $Ge = 0.5$ compared to that for $Ge = 2$ (Fig. 5). Such a diversion is due to the very steep increase of the neutral stability value of Pe in the limit $k \rightarrow 0$ when Ge decreases below 2.

A more systematic study of the effects of the inclination angle, φ , on the instability threshold is carried out by testing the dependence of the critical Péclet number on this angle. Together with the huge values of Ge considered in Figs. 5 and 6, smaller and gradually more realistic values of Ge are considered in Fig. 7. This figure shows the change of Pe_c with φ for oblique modes. The change is monotonic with the case $\varphi = \pi/2$ (longitudinal modes) displaying the minimum value of Pe_c , in all case examined. This means that the statement that longitudinal modes are those selected at onset of instability can be assumed of a general validity. Figure 7 reveals that the sensitivity of Pe_c to φ becomes stronger as Ge decreases. Another important fact is that the critical value of Pe is

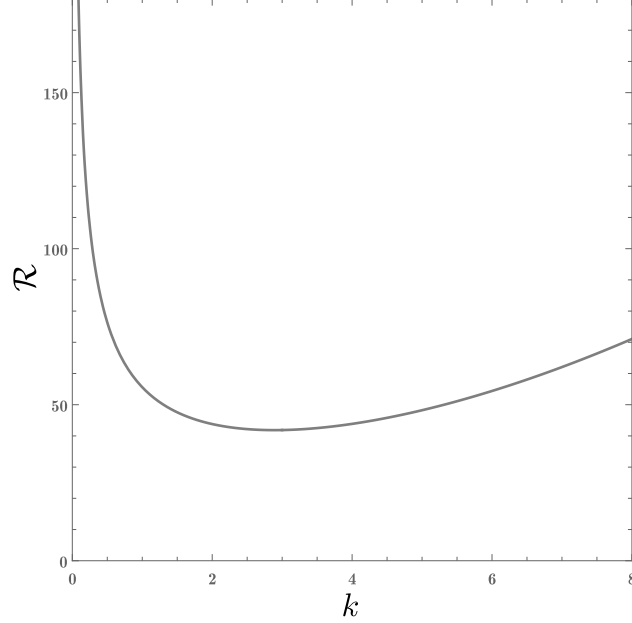


Figure 8: Longitudinal modes: neutral stability curve in the (k, \mathcal{R}) plane for the asymptotic condition $\text{Ge} \rightarrow 0$

achieved with either $k_c = 0$ or $k_c \neq 0$ for different ranges of φ . Indeed, such a complicated trend is a peculiarity for those cases where Ge is very large, $\sqrt{15}$ or 2 among the values examined in Fig. 7. For smaller Gebhart numbers, the critical conditions are always associated with $k_c \neq 0$ for every φ .

5.2 The Longitudinal Modes

Since we established that the longitudinal modes identify the onset of the instability, we will now restrict our attention to these modes. Then, the stability eigenvalue problem (25) is greatly simplified,

$$\hat{W}'''' - 2k^2 \hat{W}'' + k^4 \hat{W} - k^2 \hat{\Theta} = 0, \quad (27a)$$

$$\hat{\Theta}'' - (k^2 - i\hat{\omega}) \hat{\Theta} - \text{Pe}^2 G'(z) \hat{W} = 0, \quad (27b)$$

$$\hat{W} = 0, \quad \hat{W}' = 0, \quad \hat{\Theta}' = 0 \quad \text{for } z = 0, 1. \quad (27c)$$

The most important feature of Eqs. (27) is that neutral stability with longitudinal modes occurs with $\hat{\omega} = \omega = 0$, where the equality $\hat{\omega} = \omega$ is a consequence of the definition (24). This feature, which can be designated as a principle of exchange of stabilities, cannot be proved rigorously though it can be inferred quite clearly from the numerical data.

5.2.1 The Limit of Small Gebhart Numbers

A physically significant asymptotic condition is associated with the double limit $\text{Ge} \rightarrow 0$ and $\text{Pe} \rightarrow \infty$ on keeping $\text{Ge Pe}^2 \sim \mathcal{O}(1)$. Beyond its mathematical formulation, this asymptotic behaviour means that with small values of Ge the neutral stability threshold for Pe scales proportionally to $\text{Ge}^{-1/2}$.

By expanding $G'(z)$ in a power series of Ge , on account of Eqs. (9) and (10) and of the choice $A = A_-$, we obtain

$$G'(z) = -36 \text{Ge} (2z^3 - 3z^2 + z) + \mathcal{O}(\text{Ge}^2). \quad (28)$$

We also introduce the parameter

$$\mathcal{R} = \text{Pe} \sqrt{\text{Ge}}. \quad (29)$$

Thus, with $\text{Ge} \rightarrow 0$ and $\mathcal{R} \sim \mathcal{O}(1)$, Eqs. (27) and (28) yield

$$\hat{W}'''' - 2k^2 \hat{W}'' + k^4 \hat{W} - k^2 \hat{\Theta} = 0, \quad (30a)$$

$$\hat{\Theta}'' - (k^2 - i\hat{\omega}) \hat{\Theta} + 36 \mathcal{R}^2 (2z^3 - 3z^2 + z) \hat{W} = 0, \quad (30b)$$

$$\hat{W} = 0, \quad \hat{W}' = 0, \quad \hat{\Theta}' = 0 \quad \text{for } z = 0, 1. \quad (30c)$$

We note that, in Eqs. (30), Ge and Pe do not appear separately but only through the parameter \mathcal{R} . Hence, the neutral stability in the limit $\text{Ge} \rightarrow 0$ can be formulated as a threshold condition for the parameter \mathcal{R} . We also point out that \mathcal{R}^2 can be interpreted as a viscous dissipation based Rayleigh number

$$\mathcal{R}^2 = \frac{g \beta \Delta T_{vd} H^3}{\nu \alpha}, \quad \text{where } \Delta T_{vd} = \frac{\mu U_0^2}{\chi}, \quad (31)$$

and Eqs. (7) and (11) have been used. Here, μ is the dynamic viscosity of the fluid and χ its thermal conductivity, while ΔT_{vd} is a dimensional temperature difference characteristic of the viscous dissipation effect.

The numerical solution of Eqs. (30) allows one to obtain the neutral stability curve in the (k, \mathcal{R}) plane for the limiting case of small- Ge , as illustrated in Fig. 8. An important feature is that, unlike the neutral stability curves for finite nonzero values of Ge shown in Figs. 5 and 6, the ordinate axis $k = 0$ is a vertical asymptote for the neutral stability curve shown in Fig. 8. In fact, the critical data for the small- Ge asymptotic solution are

$$k_c = 2.88872, \quad \mathcal{R}_c = 41.8534 \quad (32)$$

Equation (32) is the basis for determining the trend of Pe_c versus Ge at small values of Ge . In particular, Eqs. (29) and (32) imply that $\text{Pe}_c \sim \mathcal{O}(\text{Ge}^{-1/2})$. This result is interesting as it differs significantly from the behaviour observed in the case of the adiabatic Darcy's flow in a porous medium [21]. In that case, it has been proved by Barletta and Rees [21] that the small- Ge trend of Pe_c is such that $\text{Pe}_c \sim \mathcal{O}(\text{Ge}^{-1})$. In other words, for Darcy's flow in a porous medium, Pe_c diverges to infinity for $\text{Ge} \rightarrow 0$ significantly faster than in the case of Newtonian flow. The reason of the difference between these cases relies in the derivative $\partial T_b / \partial z$, which drives the instability for longitudinal modes. As $\text{Ge} \rightarrow 0$, one can infer from Eqs. (8), (9) and (10) with $A = A_-$ that $\partial T_b / \partial z \sim \mathcal{O}(\text{Ge} \text{Pe}^2)$. The corresponding result in the case of Darcy's flow is $\partial T_b / \partial z \sim \mathcal{O}(\text{Ge}^2 \text{Pe}^2)$ as demonstrated in Barletta and Rees [21].

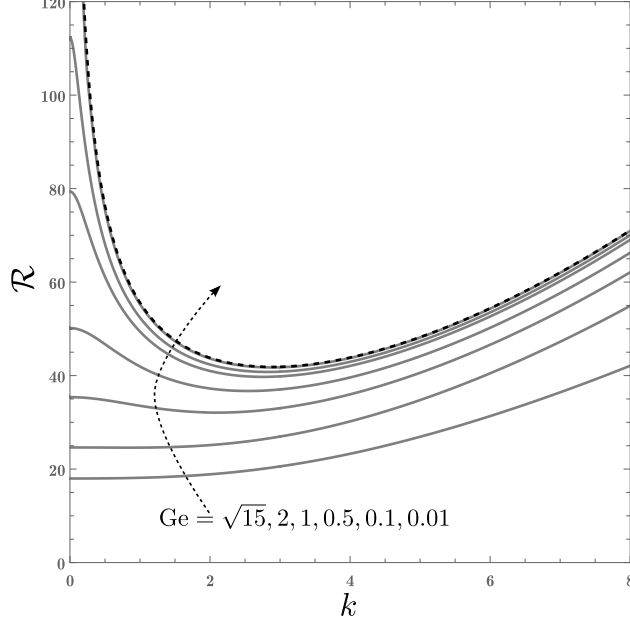


Figure 9: Longitudinal modes: neutral stability curves in the (k, \mathcal{R}) plane for different values of Ge . The dashed neutral stability curve indicates the asymptotic condition $Ge \rightarrow 0$

5.2.2 The Neutral Stability Condition for $k \rightarrow 0$

It has been pointed out that, for every $Ge \neq 0$, the neutral stability condition for longitudinal modes suggests a finite value of Pe for infinite wavelength modes, *i.e.*, for the limit $k \rightarrow 0$. This conjectured trend can be verified analytically by employing a power series solution of the eigenvalue problem (27). We set $\hat{\omega} = 0$ and adopt the expansions in even powers of k given by

$$\begin{aligned}\hat{W}(z) &= \hat{W}_0(z) + \hat{W}_2(z) k^2 + \hat{W}_4(z) k^4 + \mathcal{O}(k^6), \\ \hat{\Theta}(z) &= \hat{\Theta}_0(z) + \hat{\Theta}_2(z) k^2 + \hat{\Theta}_4(z) k^4 + \mathcal{O}(k^6), \\ Pe &= Pe_0 + Pe_2 k^2 + Pe_4 k^4 + \mathcal{O}(k^6).\end{aligned}\tag{33}$$

By substituting Eq. (33) into Eqs. (27) we obtain, to zero order in k ,

$$\hat{W}_0'''' = 0,\tag{34a}$$

$$\hat{\Theta}_0'' - Pe_0^2 G'(z) \hat{W}_0 = 0,\tag{34b}$$

$$\begin{aligned}\hat{W}_0(0) &= 0, & \hat{W}_0'(0) &= 0, & \hat{\Theta}_0'(0) &= 0, \\ \hat{W}_0(1) &= 0, & \hat{W}_0'(1) &= 0, & \hat{\Theta}_0'(1) &= 0.\end{aligned}\tag{34c}$$

The solution of Eqs. (34) is

$$\hat{W}_0(z) = 0, \quad \hat{\Theta}_0(z) = 1,\tag{35}$$

while Pe_0 remains yet undetermined.

Indeed, $\hat{\Theta}_0(z)$ could be equal to any constant value as the original problem (27) is homogeneous. Choosing the constant value 1 in Eq. (35) means getting rid of the scale invariance for the eigenfunctions by implicitly fixing the extra condition $\hat{\Theta}(0) = 1$. The immediate consequence is that

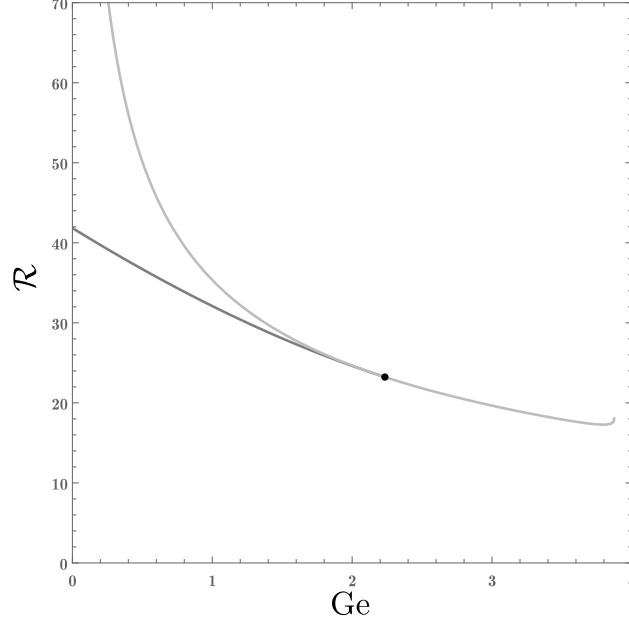


Figure 10: Longitudinal modes: \mathcal{R}_c versus Ge (dark grey line) compared with \mathcal{R}_0 versus Ge (light grey line). The black dot denotes the transition from $k_c \neq 0$ to $k_c = 0$ occurring when Ge is given by Eq. (40)

$\hat{\Theta}_n(0) = 0$ for every positive integer n . Therefore, the system obtained from Eqs. (27) to second order in k is given by

$$\hat{W}_2'''' - 1 = 0, \quad (36a)$$

$$\hat{\Theta}_2'' - 1 - Pe_0^2 G'(z) \hat{W}_2 = 0, \quad (36b)$$

$$\hat{W}_2(0) = 0, \quad \hat{W}_2'(0) = 0, \quad \hat{\Theta}_2(0) = 0, \quad \hat{\Theta}_2'(0) = 0,$$

$$\hat{W}_2(1) = 0, \quad \hat{W}_2'(1) = 0. \quad (36c)$$

There should also be an extra condition $\hat{\Theta}_2'(1) = 0$, but it is not needed to determine the solution of Eqs. (36). We do not report such a solution for the sake of brevity. We just say that $\hat{W}_2(z)$ is a fourth-degree polynomial in z , while $\hat{\Theta}_2(z)$ is an eleventh-degree polynomial in z .

Forcing the extra condition $\hat{\Theta}_2'(1) = 0$ results in a relation between Pe_0 and Ge , namely

$$Pe_0 = 2 \sqrt{\frac{105 Ge^2}{(20 - Ge^2) \sqrt{15(15 - Ge^2)} + 25 Ge^2 - 300}}. \quad (37)$$

A characteristic feature of Eq. (37) is that $Pe_0 \sim \mathcal{O}(Ge^{-2})$ in the limit $Ge \rightarrow 0$. This feature justifies our statement in Section 5.2.1 that the ordinate axis $k = 0$ is a vertical asymptote for the neutral stability curve when $Ge \rightarrow 0$. Equation 37 provides also a rigorous evaluation of the critical Péclet number in the maximum- Ge case, *i.e.*, for $Ge = \sqrt{15}$. In fact, $k_c = 0$ in this case and

$$Pe_c = Pe_0 = 2\sqrt{21} \approx 9.16515. \quad (38)$$

By comparing this result with the numerical value of Pe along the neutral stability curve (see Fig. 5) with $k = 0.01$, we estimate a relative discrepancy less than 0.01%. Such a discrepancy is extremely satisfactory, given that the numerical shooting-method solver employed for the eigenvalue problem (27) yields the smallest accuracy when k is close to 0.

By considering the system obtained from Eqs. (27) to fourth order in k , one obtains

$$\hat{W}_4'''' - 2\hat{W}_2'' - \hat{\Theta}_2 = 0, \quad (39a)$$

$$\hat{\Theta}_4'' - \hat{\Theta}_2 - \left(Pe_0^2 \hat{W}_4 + 2Pe_0 Pe_2 \hat{W}_2 \right) G'(z) = 0, \quad (39b)$$

$$\begin{aligned} \hat{W}_4(0) = 0, \quad \hat{W}_4'(0) = 0, \quad \hat{\Theta}_4(0) = 0, \quad \hat{\Theta}_4'(0) = 0, \\ \hat{W}_4(1) = 0, \quad \hat{W}_4'(1) = 0. \end{aligned} \quad (39c)$$

The extra condition $\hat{\Theta}_4'(1) = 0$ yields a relation between Pe_2 and Ge . We do not report the analytical expression of Pe_2 , but we just note that it can be used to detect the threshold for k_c to change from zero to nonzero as Ge increases. We already pointed out that the neutral stability curve for longitudinal modes with $Ge = 2$ has $k_c \neq 0$, while that for $Ge = \sqrt{15}$ has $k_c = 0$. The threshold value of Ge where k_c changes from a nonzero to a zero value can be detected as that value corresponding to a change in the concavity of the neutral stability curve at $k = 0$. Such a change in concavity corresponds to a change of sign for Pe_2 . In fact, the condition $Pe_2 = 0$ yields

$$Ge = 2.23397. \quad (40)$$

5.2.3 The Neutral Stability Curves and the Critical Values

The neutral stability curves for longitudinal modes represented in the (k, \mathcal{R}) plane are reported in Fig. 9 for decreasing values of Ge ranging from its maximum, $\sqrt{15}$, to 0.01. The neutral stability curve for the asymptotic case $Ge \rightarrow 0$ (dashed line) is reported for comparison. The first impression is that the neutral stability curve for $Ge = 0.01$ matches almost perfectly that for $Ge \rightarrow 0$. However, by employing Eq. (37), one should keep in mind that the neutral stability curve for $Ge = 0.01$ yields a finite, though very large, value of \mathcal{R} in the limit $k \rightarrow 0$, *i.e.* $\mathcal{R} = 354.967$, while the neutral stability curve for the asymptotic case $Ge \rightarrow 0$ has a vertical asymptote at $k = 0$.

Figure 10 displays a comparison between the critical value of \mathcal{R} and the $k \rightarrow 0$ limiting value of \mathcal{R} versus Ge . In fact, for a given Ge , we define

$$\mathcal{R}_c = Pe_c \sqrt{Ge}, \quad \mathcal{R}_0 = Pe_0 \sqrt{Ge}. \quad (41)$$

A dark grey line is employed for \mathcal{R}_c and a light grey line for \mathcal{R}_0 . The latter line almost overlaps the former when Ge is greater than 2, while the exact overlapping occurs when Ge exceeds the threshold value given by Eq. (40) and identified in Fig. 10 by a black dot. The reason is that the difference between \mathcal{R}_c and \mathcal{R}_0 becomes very small when Ge is so large. When $Ge \rightarrow 0$, the value of \mathcal{R}_c agrees with that given by Eq. (32). When $Ge = \sqrt{15} \approx 3.87298$, both the lines come to an end as this value of Ge is the maximum possible for the existence of the basic state. Although hardly significant for a physical system, the range of Ge very close to its maximum shows a diversion from the general decreasing trend of both \mathcal{R}_c and \mathcal{R}_0 versus Ge with a minimum which can be accurately evaluated for \mathcal{R}_0 by using Eq. (37),

$$\mathcal{R}_{0,\min} = 3\sqrt{21\sqrt{\frac{5}{2}}} \approx 17.2869, \quad Ge_{\min} = 6\sqrt{\frac{2}{5}} \approx 3.79473. \quad (42)$$

| Ge | k_c | Pe _c | \mathcal{R}_c | Pe ₀ | \mathcal{R}_0 |
|-------------|---------|-----------------|-----------------|-----------------|-----------------|
| 0 | 2.88872 | ∞ | 41.8534 | ∞ | ∞ |
| 0.01 | 2.88237 | 417.4493 | 41.7449 | 3549.6464 | 354.9646 |
| 0.1 | 2.82398 | 128.9560 | 40.7795 | 354.9500 | 112.2450 |
| 0.2 | 2.75634 | 88.8359 | 39.7286 | 177.4528 | 79.3593 |
| 0.3 | 2.68571 | 70.6563 | 38.7001 | 118.2772 | 64.7831 |
| 0.4 | 2.61199 | 59.5981 | 37.6932 | 88.6819 | 56.0874 |
| 0.5 | 2.53508 | 51.9123 | 36.7076 | 70.9188 | 50.1472 |
| 0.8 | 2.28435 | 37.8763 | 33.8776 | 44.2515 | 39.5797 |
| 1 | 2.09952 | 32.0986 | 32.0986 | 35.3470 | 35.3470 |
| 1.2 | 1.89924 | 27.7601 | 30.4097 | 29.4002 | 32.2063 |
| 1.5 | 1.56474 | 22.9062 | 28.0543 | 23.4372 | 28.7045 |
| 1.8 | 1.17077 | 19.3205 | 25.9212 | 19.4448 | 26.0879 |
| 2 | 0.84224 | 17.4116 | 24.6237 | 17.4397 | 24.6634 |
| 2.2 | 0.31397 | 15.7919 | 23.4232 | 15.7924 | 23.4239 |
| 2.23397 | 0 | 15.5412 | 23.2286 | 15.5412 | 23.2286 |
| $\sqrt{15}$ | 0 | 9.1652 | 18.0369 | 9.1652 | 18.0369 |

Table 1: Values of k_c , Pe_c, \mathcal{R}_c , Pe₀, \mathcal{R}_0 versus Ge

Table 1 reports the critical data for the parameters k , Pe and \mathcal{R} for several Gebhart numbers, together with the corresponding values of Pe and \mathcal{R} obtained by employing the $k \rightarrow 0$ asymptotic solution Eq. (37). The first row of this table, for Ge = 0, is relative to the asymptotic solution discussed in Section 5.2.1. We note that the discrepancy between the asymptotic case Ge \rightarrow 0 and the case Ge = 0.01 is less than 0.3% both in terms of k_c and \mathcal{R}_c . This means that, for practical purposes, the asymptotic solution for Ge \rightarrow 0 can be safely employed for all cases with Ge \leq 0.01. In Table 1, we also reported the threshold value of Ge defined by Eq. (40) above which $k_c = 0$.

Even if we declared that the focus of our stability analysis is on the $A = A_-$ branch, a sample comparison between the stability characteristics of dual flows for a given Gebhart number could be interesting. Thus, we have selected a case, Ge = 3.8, very close to the maximum, Ge = $\sqrt{15}$, so that the dual branches are not too different. We recall that the basic dual flows for Ge = 3.8 are illustrated in Figs. 1 and 3 and commented on in Section 3. The neutral stability curves relative to both the dual branches with Ge = 3.8 are displayed in Fig. 11 for transverse modes and for longitudinal modes. In both dual branches, the longitudinal modes are the most unstable. However, the $A = A_-$ branch displays a critical value of Pe smaller than the critical value for the $A = A_+$ branch. Then, the $A = A_-$ is more unstable than the $A = A_+$ branch in this case. This outcome is not surprising as a similar behaviour was observed in a similar previous studies dealing with Darcy's flow in a porous channel [21]. A minor aspect clearly visible in Fig. 11 is that the onset of instability with longitudinal modes, for the $A = A_+$ branch, happens with a nonzero wavenumber mode, On the other hand, $k_c = 0$ for the $A = A_-$ branch.

6 Conclusions

The onset of convective instability for the buoyant parallel flows in a horizontal plane channel with adiabatic walls has been studied. The action of buoyancy and the unstable behaviour are induced

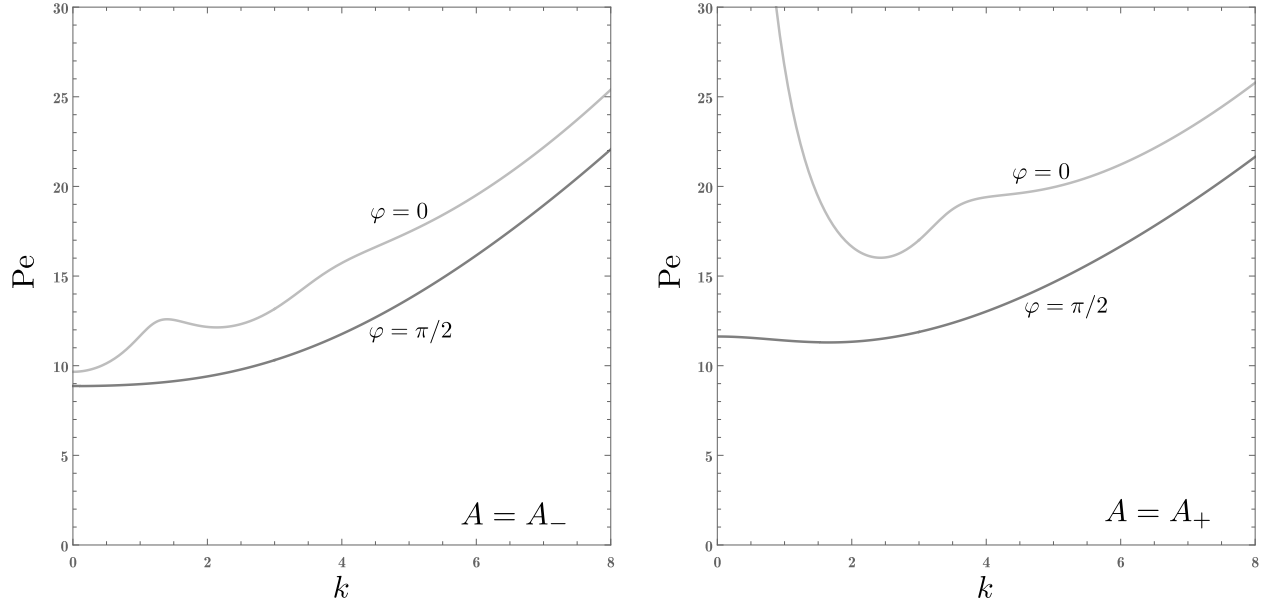


Figure 11: Neutral stability curves for $Ge = 3.8$ in the (k, Pe) plane for transverse (light grey line, $\varphi = 0$) and longitudinal (dark grey line, $\varphi = \pi/2$) modes. Both dual branches $A = A_-$ and $A = A_+$ are considered

by the viscous dissipation for a flow with a given mass flow rate.

The main features and, in particular, the duality of the basic parallel flows have been surveyed. The stability analysis has been focussed on the lower branch of the dual flows, as the higher branch turned out to display features utterly incompatible with the Oberbeck-Boussinesq approximation. The governing dimensionless parameters for the dual flows are the Gebhart number, Ge , also known as the dissipation number, and the Péclet number, Pe .

The stability analysis has been formulated by evaluating the neutrally stable value of Pe for a given Ge . Since the dual flows are mathematically defined only with $Ge \leq \sqrt{15}$, this whole parametric range has been explored. However, it has been also mentioned that values of Ge as large as its maximum are hardly significant for any real-world application, even over length scales of geophysical interest Barletta et al. [18].

The linear stability analysis has been formulated by assuming creeping flow, which means an infinite Prandtl number. Such an analysis has been carried out through a numerical solution of the stability eigenvalue problem obtained by the shooting method. The main results of the stability analysis can be summarised as follows:

- The preferred perturbation modes causing the transition to instability are longitudinal, for every value of Ge . The reaction of the base flows to arbitrary oblique perturbation modes has been tested by defining the inclination angle φ between the base flow direction and the wave vector corresponding to the oblique modes. Then, the inclination angle has been varied in the range $0 \leq \varphi \leq \pi/2$, with $\varphi = 0$ identifying the transverse modes and $\varphi = \pi/2$ defining the longitudinal modes. The value $\varphi = \pi/2$ always yields the least stable condition.
- The analysis of the neutral stability condition for the longitudinal modes reveals that such modes are non-travelling as their angular frequency and, hence, their phase velocity is always

zero. The critical values of either Pe or the parameter $\mathcal{R} = Pe\sqrt{Ge}$ are generally decreasing functions of Ge , except for a very narrow range close to the maximum $Ge = \sqrt{15}$. The longitudinal modes with a zero wavenumber, or an infinite wavelength, have a finite neutrally stable value of Pe for any nonzero Ge . This regime has been studied via an analytical asymptotic solution.

- A physically important situation is one where Ge is negligibly small, the Péclet number is very large, but the parameter \mathcal{R} remains finite. For this limiting case, the critical condition for the onset of the instability has been evaluated as $\mathcal{R}_c = 41.8534$.

The study of the instability induced by the viscous dissipation has been carried out in this paper by assuming conditions of creeping flow where the Prandtl number is prescribed to be extremely large though maintaining a finite Péclet number. With this scenario in mind, the viscous dissipation instability is one emerging at very small Reynolds numbers and, hence, has likely no interrelation with the hydrodynamic instability analysed through the solution of the Orr-Sommerfeld problem. The extension of our study to a hybrid parametric domain where a finite Prandtl number is assumed can be a challenge for future investigations. Such a development can offer a chance to test the interplay between the viscous dissipation instability and the Orr-Sommerfeld hydrodynamic instability in a plane parallel channel.

Acknowledgement

The authors acknowledge financial support from Italian Ministry of Education, University and Research (MIUR) grant number PRIN 2017F7KZWS.

References

- [1] P. G. Drazin, W. H. Reid, *Hydrodynamic Stability*, 2nd Edition, Cambridge University Press, 2004.
- [2] P. K. Kundu, I. M. Cohen, D. R. Dowling, *Fluid Mechanics*, 6th Edition, Academic Press, 2016.
- [3] D. D. Joseph, Variable viscosity effects on the flow and stability of flow in channels and pipes, *The Physics of Fluids* 7 (1964) 1761–1771.
- [4] D. D. Joseph, Stability of frictionally-heated flow, *The Physics of Fluids* 8 (1965) 2195–2200.
- [5] A. Barletta, D. A. Nield, Convection-dissipation instability in the horizontal plane Couette flow of a highly viscous fluid, *Journal of Fluid Mechanics* 662 (2010) 475–492.
- [6] A. Barletta, M. Celli, D. A. Nield, On the onset of dissipation thermal instability for the Poiseuille flow of a highly viscous fluid in a horizontal channel, *Journal of Fluid Mechanics* 681 (2011) 499–514.
- [7] A. Barletta, On the thermal instability induced by viscous dissipation, *International Journal of Thermal Sciences* 88 (2015) 238–247.

- [8] M. Miklavčič, Stability analysis of some fully developed mixed convection flows in a vertical channel, *ZAMM-Journal of Applied Mathematics and Mechanics/Zeitschrift für Angewandte Mathematik und Mechanik* 95 (2015) 982–986.
- [9] A. Barletta, M. Miklavčič, On fully developed mixed convection with viscous dissipation in a vertical channel and its stability, *ZAMM-Journal of Applied Mathematics and Mechanics/Zeitschrift für Angewandte Mathematik und Mechanik* 96 (2016) 1457–1466.
- [10] L. A. Lund, Z. Omar, I. Khan, S. Kadry, S. Rho, I. A. Mari, K. S. Nisar, Effect of viscous dissipation in heat transfer of MHD flow of micropolar fluid partial slip conditions: dual solutions and stability analysis, *Energies* 12 (24) (2019) 4617.
- [11] Y. Requilé, S. C. Hirata, M. N. Ouarzazi, A. Barletta, Weakly nonlinear analysis of viscous dissipation thermal instability in plane Poiseuille and plane Couette flows, *Journal of Fluid Mechanics* 886.
- [12] L. A. Lund, Z. Omar, J. Raza, I. Khan, Magnetohydrodynamic flow of Cu-Fe₃O₄/H₂O hybrid nanofluid with effect of viscous dissipation: dual similarity solutions, *Journal of Thermal Analysis and Calorimetry* 143 (2021) 915–927.
- [13] E. V. M. Reis, L. S. de B. Alves, Convective and absolute instabilities induced by viscous dissipation in the thermocapillary convection with through-flow, *ASME Journal of Heat Transfer* 143 (2021) 052601.
- [14] A. Barletta, G. Mulone, The energy method analysis of the Darcy-Bénard problem with viscous dissipation, *Continuum Mechanics and Thermodynamics* 33 (2021) 25–33.
- [15] K. Ali Amar, S. C. Hirata, M. N. Ouarzazi, Soret effect on the onset of viscous dissipation thermal instability for Poiseuille flows in binary mixtures, *Physics of Fluids* 34 (2022) 114101.
- [16] D. L. Turcotte, D. A. Spence, H. H. Bau, Multiple solutions for natural convective flows in an internally heated, vertical channel with viscous dissipation and pressure work, *International Journal of Heat and Mass Transfer* 25 (1982) 699–706.
- [17] A. Barletta, E. Magyari, B. Keller, Dual mixed convection flows in a vertical channel, *International Journal of Heat and Mass Transfer* 48 (2005) 4835–4845.
- [18] A. Barletta, M. Celli, P. V. Brandão, On mixed convection in a horizontal channel, viscous dissipation and flow duality, *Fluids* 7 (5) (2022) 170.
- [19] G. Wilks, J. S. Bramley, Dual solutions in mixed convection, *Proceedings of the Royal Society of Edinburgh: Section A Mathematics* 87 (1981) 349–358.
- [20] K. Naganthran, M. Mustafa, A. Mushtaq, R. Nazar, Dual solutions for fluid flow over a stretching/shrinking rotating disk subject to variable fluid properties, *Physica A: Statistical Mechanics and Its Applications* 556 (2020) 124773.
- [21] A. Barletta, D. A. S. Rees, Stability analysis of dual adiabatic flows in a horizontal porous layer, *International Journal of Heat and Mass Transfer* 52 (2009) 2300–2310.

- [22] B. Gebhart, Effects of viscous dissipation in natural convection, *Journal of Fluid Mechanics* 14 (1962) 225–232.
- [23] C. Kincaid, P. Silver, The role of viscous dissipation in the orogenic process, *Earth and Planetary Science Letters* 142 (1996) 271–288.
- [24] A. P. van den Berg, D. A. Yuen, The role of shear heating in lubricating mantle flow, *Earth and planetary science letters* 151 (1997) 33–42.
- [25] B. Straughan, *The Energy Method, Stability, and Nonlinear Convection*, Springer, 2013.
- [26] A. Barletta, *Routes to Absolute Instability in Porous Media*, Springer, 2019.
- [27] H. Park, L. Sirovich, Hydrodynamic stability of Rayleigh-Bénard convection with constant heat flux boundary condition, *Quarterly of Applied Mathematics* 49 (1991) 313–332.